APPLIED SCIENCES AND ENGINEERING

Ultratransparent and stretchable graphene electrodes

Nan Liu,[1]* Alex Chortos,[1]* Ting Lei,[1]* Lihua Jin,[2] Taeho Roy Kim,[3] Won-Gyu Bae,[1] Chenxin Zhu,[4] Sihong Wang,[1] Raphael Pfattner,[1] Xiyuan Chen,[5] Robert Sinclair,[3] Zhenan Bao[1]†

Two-dimensional materials, such as graphene, are attractive for both conventional semiconductor applications and nascent applications in flexible electronics. However, the high tensile strength of graphene results in fracturing at low strain, making it challenging to take advantage of its extraordinary electronic properties in stretchable electronics. To enable excellent strain-dependent performance of transparent graphene conductors, we created graphene nanoscrolls in between stacked graphene layers, referred to as multilayer graphene/graphene scrolls (MGGs). Under strain, some scrolls bridged the fragmented domains of graphene to maintain a percolating network that enabled excellent conductivity at high strains. Trilayer MGGs supported on elastomers retained 65% of their original conductance at 100% strain, which is perpendicular to the direction of current flow, whereas trilayer films of graphene without nanoscrolls retained only 25% of their starting conductance. A stretchable all-carbon transistor fabricated using MGGs as electrodes exhibited a transmittance of >90% and retained 60% of its original current output at 120% strain (parallel to the direction of charge transport). These highly stretchable and transparent all-carbon transistors could enable sophisticated stretchable optoelectronics.

INTRODUCTION

Stretchable transparent electronics is a growing field that has important applications in advanced biointegrated systems (*1*, *2*) as well as the potential to integrate with stretchable optoelectronics (*3*, *4*) to produce sophisticated soft robotics and displays. Graphene exhibits highly desirable properties of atomic thickness, high transparency, and high conductivity, but its implementation in stretchable applications has been inhibited by its tendency to crack at small strains. Overcoming the mechanical limitations of graphene could enable new functionality in stretchable transparent devices.

The unique properties of graphene make it a strong candidate for the next generation of transparent conductive electrodes (*5*, *6*). Compared with the most commonly used transparent conductor, indium tin oxide [ITO; 100 ohms/square (sq) at 90% transparency], monolayer graphene grown by chemical vapor deposition (CVD) has a similar combination of sheet resistance (125 ohms/sq) and transparency (97.4%) (*5*). In addition, graphene films have extraordinary flexibility compared to ITO (*7*). For example, on a plastic substrate, its conductance can be retained even for a bending radius of curvature as small as 0.8 mm (*8*). To further enhance its electrical performance as a transparent flexible conductor, previous works have developed graphene hybrid materials with one-dimensional (1D) silver nanowires or carbon nanotubes (CNTs) (*9*–*11*). Moreover, graphene has been used as electrodes for mixed dimensional heterostructural semiconductors (such as 2D bulk Si, 1D nanowires/nanotubes, and 0D quantum dots) (*12*), flexible transistors, solar cells, and light-emitting diodes (LEDs) (*13*–*23*).

Although graphene has shown promising results for flexible electronics, its application in stretchable electronics has been limited by its mechanical properties (*17*, *24*, *25*); graphene has an in-plane stiffness of 340 N/m and a Young's modulus of 0.5 TPa (*26*). The strong carbon-carbon network does not provide any energy dissipation mechanisms for applied strain and therefore readily cracks at less than 5% strain. For example, CVD graphene transferred onto a polydimethylsiloxane (PDMS) elastic substrate can only maintain its conductivity at less than 6% strain (*8*). Theoretical calculations show that crumpling and interplay between different layers should strongly decrease the stiffness (*26*). By stacking graphene into multiple layers, it is reported that this bi- or trilayer graphene is stretchable to 30% strain, exhibiting resistance change 13 times smaller than that of monolayer graphene (*27*). However, this stretchability is still significantly inferior to state-of-the-art stretchable conductors (*28*, *29*).

Transistors are important in stretchable applications because they enable sophisticated sensor readout and signal analysis (*30*, *31*). Transistors on PDMS with multilayer graphene as source/drain electrodes and channel material can maintain electrical function up to 5% strain (*32*), which is significantly below the minimum required value (~50%) for wearable health-monitoring sensors and electronic skin (*33*, *34*). Recently, a graphene kirigami approach has been explored, and the transistor gated by a liquid electrolyte can be stretched to as much as 240% (*35*). However, this method requires suspended graphene, which complicates the fabrication process.

Here, we achieve highly stretchable graphene devices by intercalating graphene scrolls (~1 to 20 μm long, ~0.1 to 1 μm wide, and ~10 to 100 nm high) in between graphene layers. We hypothesize that these graphene scrolls could provide conductive paths to bridge cracks in the graphene sheets, thus maintaining high conductivity under strain. The graphene scrolls do not require additional synthesis or process; they are naturally formed during the wet transfer procedure. By using multilayer G/G (graphene/graphene) scrolls (MGGs) graphene stretchable electrodes (source/drain and gate) and semiconducting CNTs, we were able to demonstrate highly transparent and highly stretchable all-carbon transistors, which can be stretched to 120% strain (parallel to the direction of charge transport) and retain 60% of their original current output. This is the most stretchable transparent carbon-based transistor so far, and it provides sufficient current to drive an inorganic LED.

RESULTS AND DISCUSSION

Fabrication of MGG structures

To enable large-area transparent stretchable graphene electrodes, we chose CVD-grown graphene on Cu foil. The Cu foil was suspended

[1]Department of Chemical Engineering, Stanford University, Stanford, CA 94305, USA. [2]Department of Civil and Environmental Engineering, Stanford University, Stanford, CA 94305, USA. [3]Department of Materials Science and Engineering, Stanford University, Stanford, CA 94305, USA. [4]Department of Electrical Engineering, Stanford University, Stanford, CA 94305, USA. [5]Department of Mechanical Engineering, Stanford University, Stanford, CA 94305, USA.
*These authors contribute equally to this work.
†Corresponding author: Email: zbao@stanford.edu

in the center of a CVD quartz tube to allow the growth of graphene on both sides, forming G/Cu/G structures. To transfer graphene, we first spin-coated a thin layer of poly(methyl methacrylate) (PMMA) to protect one side of the graphene, which we named topside graphene (vice versa for the other side of the graphene), and subsequently, the entire film (PMMA/top graphene/Cu/bottom graphene) was soaked in $(NH_4)_2S_2O_8$ solution to etch away the Cu foil. The bottom-side graphene without the PMMA coating will unavoidably have cracks and defects that allow an etchant to penetrate through (*36*, *37*). As illustrated in Fig. 1A, under the effect of surface tension, the released graphene domains rolled up into scrolls and subsequently attached onto the remaining top-G/PMMA film. The top-G/G scrolls could be transferred onto any substrate, such as SiO_2/Si, glass, or soft polymer. Repeating this transfer process several times onto the same substrate gives MGG structures.

To verify that the scrolls are rolled graphene in nature, we conducted high-resolution transmission electron microscopy (TEM) and electron energy loss (EEL) spectroscopy studies on the monolayer top-G/G scroll structures. Figure 1B shows the hexagonal structure of a monolayer graphene, and the inset is an overall morphology of the film covered on a single carbon hole of the TEM grid. The monolayer graphene spans most of the grid, and some graphene flakes in the presence of multiple stacks of hexagonal rings appear (Fig. 1B). By zooming into an individual scroll (Fig. 1C), we observed a large amount of graphene lattice fringes, with the lattice spacing in the range of 0.34 to 0.41 nm. These measurements suggest that the flakes are randomly rolled up and are not perfect graphite, which has a lattice spacing of 0.34 nm in "ABAB" layer stacking. Figure 1D shows the carbon K-edge EEL spectrum, where the peak at 285 eV originates from the π* orbital and the other one around 290 eV is due to the transition of the σ* orbital. It can be seen that sp^2 bonding dominates in this structure, verifying that the scrolls are highly graphitic.

Morphological and electrical characterizations of MGGs

Optical microscopy and atomic force microscopy (AFM) images provide insight into the distribution of graphene nanoscrolls in the MGGs (Fig. 1, E to G, and figs. S1 and S2). The scrolls are randomly distributed over the surface, and their in-plane density increases proportionally to the number of stacked layers. Many scrolls are tangled into knots and exhibit nonuniform heights in the range of 10 to 100 nm. They are 1 to 20 μm long and 0.1 to 1 μm wide, depending on the sizes

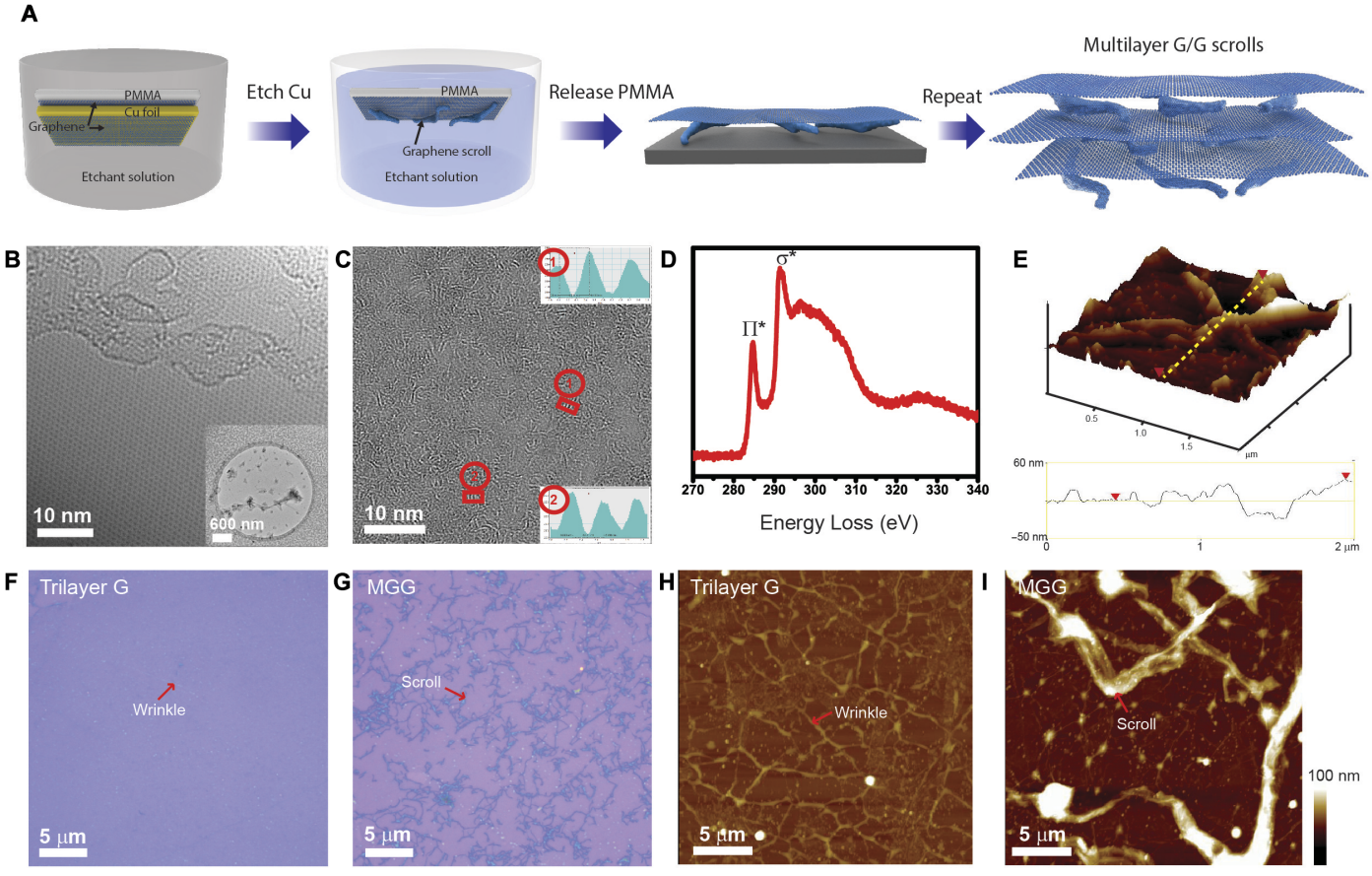

Fig. 1. Schematic illustrations and morphological characterizations of MGGs. (**A**) Schematic illustration of the fabrication procedure for MGGs as a stretchable electrode. During the graphene transfer, backside graphene on Cu foil was broken at boundaries and defects, rolled up into arbitrary shapes, and tightly attached onto the upper films, forming nanoscrolls. The fourth cartoon depicts the stacked MGG structure. (**B** and **C**) High-resolution TEM characterizations of a monolayer MGG, focusing on the monolayer graphene (B) and the scroll (C) region, respectively. The inset of (B) is a low-magnification image showing the overall morphology of monolayer MGGs on the TEM grid. Insets of (C) are the intensity profiles taken along the rectangular boxes indicated in the image, where the distances between the atomic planes are 0.34 and 0.41 nm. (**D**) Carbon K-edge EEL spectrum with the characteristic graphitic π* and σ* peaks labeled. (**E**) Sectional AFM image of monolayer G/G scrolls with a height profile along the yellow dotted line. (**F** to **I**) Optical microscopy and AFM images of trilayer G without (F and H) and with scrolls (G and I) on 300-nm-thick SiO_2/Si substrates, respectively. Representative scrolls and wrinkles were labeled to highlight their differences.

of their initial graphene flakes. As shown in Fig. 1 (H and I), the scrolls have significantly larger sizes than the wrinkles, leading to a much rougher interface in between graphene layers.

To measure the electrical properties, we patterned graphene films with or without scroll structures and layer stacking into 300-μm-wide and 2000-μm-long strips using photolithography. Two-probe resistances as a function of strain were measured under ambient conditions. The presence of scrolls reduced the resistivity for monolayer graphene by 80% with only a 2.2% decrease in the transmittance (fig. S4). This confirms that nanoscrolls, which have a high current density up to 5×10^7 A/cm^2 (*38*, *39*), make a very positive electrical contribution to the MGGs. Among all the mono-, bi-, and trilayer plain graphene and MGGs, the trilayer MGG has the best conductance with a transparency of almost 90%. To compare with other sources of graphene reported in the literature, we also measured four-probe sheet resistances (fig. S5) and listed them as a function of transmittance at 550 nm (fig. S6) in Fig. 2A. MGG shows comparable or higher conductivity and transparency than artificially stacked multilayer plain graphene and reduced graphene oxide (RGO) (*6*, *8*, *18*). Note that the sheet resistances of artificially stacked multilayer plain graphene from literature are slightly higher than that of our MGG, probably because of their unoptimized growth conditions and transfer method.

To evaluate the strain-dependent performance of the MGG, we transferred graphene onto thermoplastic elastomer styrene-ethylene-butadiene-styrene (SEBS) substrates (~2 cm wide and ~5 cm long), and the conductivity was measured as the substrate was stretched (see Materials and Methods) both perpendicular and parallel to the direction of current flow (Fig. 2, B and C). The strain-dependent electrical behavior improved with the incorporation of nanoscrolls and increasing numbers of graphene layers. For example, when strain is perpendicular to current flow, for monolayer graphene, the addition of scrolls increased the strain at electrical breakage from 5 to 70%. The strain tolerance of the trilayer graphene is also significantly improved compared with the monolayer graphene. With nanoscrolls, at 100% perpendicular strain, the resistance of the trilayer MGG structure only increased by 50%, in comparison to 300% for trilayer graphene without scrolls. Resistance change under cyclic strain loading was investigated. For comparison (Fig. 2D), the resistances of a plain bilayer graphene film increased about 7.5 times after ~700 cycles at 50% perpendicular strain and kept increasing with strain in each cycle. On the other hand, the resistance of a bilayer MGG only increased about 2.5 times after ~700 cycles. Applying up to 90% strain along the parallel direction, the resistance of trilayer graphene increased ~100 times after 1000 cycles, whereas it is only ~8 times in a trilayer MGG (Fig. 2E). Cycling results are shown in fig. S7. The relatively faster increase in resistance along the parallel strain direction is because the orientation of cracks is perpendicular to the direction of current flow. The deviation of resistance during loading and unloading strain is due to the viscoelastic

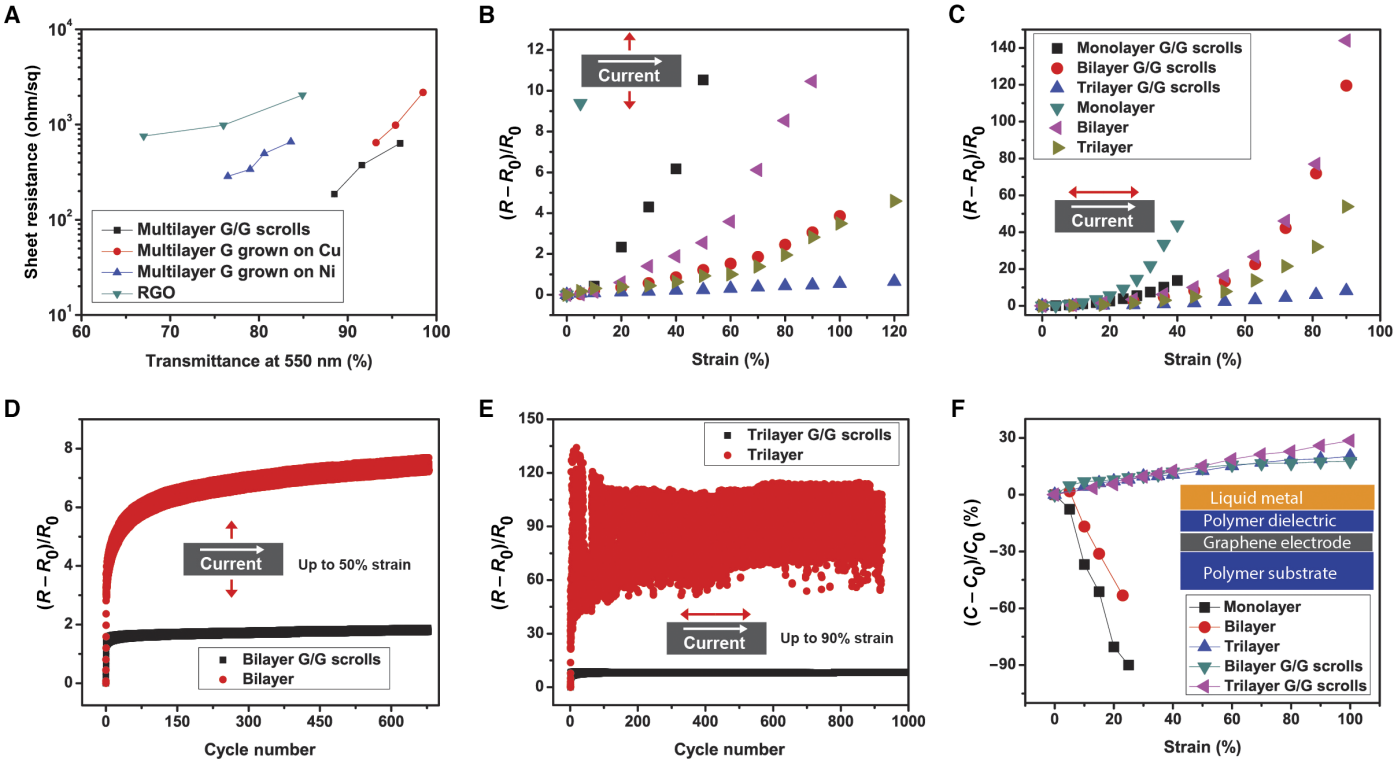

Fig. 2. Comparison of electrical and optical properties of MGGs and graphene. (**A**) Four-probe sheet resistances versus transmittance at 550 nm for several types of graphene, where black squares denote mono-, bi-, and trilayer MGGs; red circles and blue triangles correspond with multilayer plain graphene grown on Cu and Ni from the studies of Li *et al.* (*6*) and Kim *et al.* (*8*), respectively, and subsequently transferred onto SiO_2/Si or quartz; and green triangles are values for RGO at different reducing degrees from the study of Bonaccorso *et al.* (*18*). (**B** and **C**) Normalized resistance change of mono-, bi- and trilayer MGGs and G as a function of perpendicular (B) and parallel (C) strain to the direction of current flow. (**D**) Normalized resistance change of bilayer G (red) and MGG (black) under cyclic strain loading up to 50% perpendicular strain. (**E**) Normalized resistance change of trilayer G (red) and MGG (black) under cyclic strain loading up to 90% parallel strain. (**F**) Normalized capacitance change of mono-, bi- and trilayer G and bi- and trilayer MGGs as a function of strain. The inset is the capacitor structure, where the polymer substrate is SEBS and the polymer dielectric layer is the 2-μm-thick SEBS.

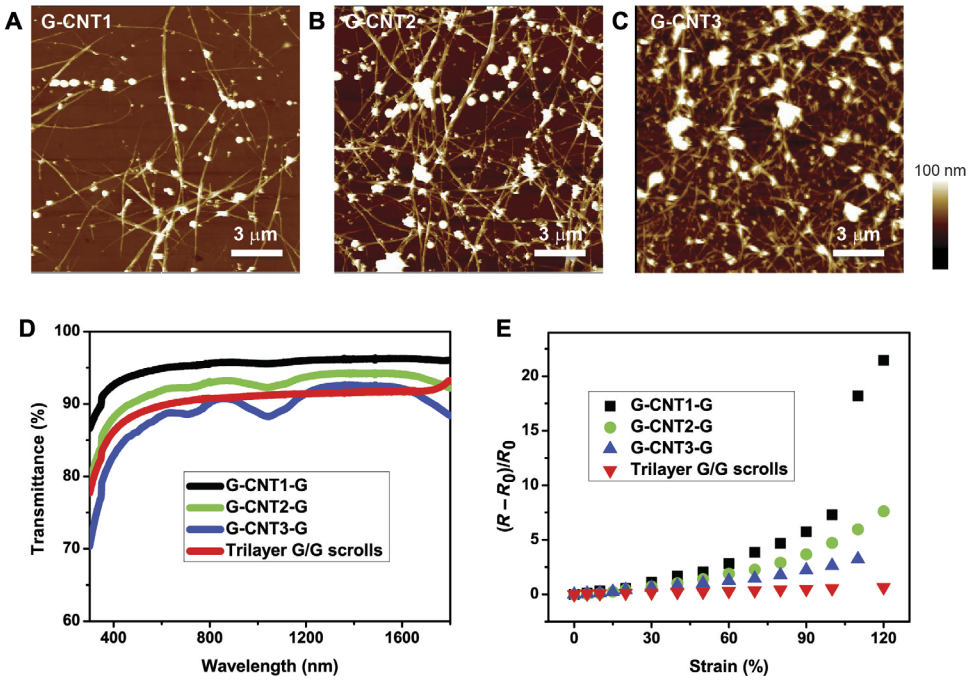

Fig. 3. Exploration of CNTs as a replacement of graphene scrolls. (**A** to **C**) AFM images of three different densities of CNTs (CNT1<CNT2<CNT3) on graphene. (**D**) Optical transmittances of G-CNT-G on quartz. (**E**) Normalized resistance change of G-CNT-G as a function of strain. Transmittance and normalized resistance change of trilayer MGGs are listed as a comparison.

Table 1. Comparison of the transmittance at 550 nm and the normalized resistance change at designated strains of the two types of graphene structures. N/A, not applicable.

	Transmittance at 550 nm (%)	$(R - R_0)/R_0$ at 50%	$(R - R_0)/R_0$ at 100%
Mono-G/G scrolls	95.9	1.96	N/A
Bi-G/G scrolls	91.6	1.22	3.86
Tri-G/G scrolls	88.5	0.24	0.54
G-CNT1-G	94.6	2.07	7.29
G-CNT2-G	91.3	1.39	4.72
G-CNT3-G	87.4	0.72	2.22

recovery of SEBS elastomer substrate. The more stable resistance of the MGG strips during cycling is due to the presence of large scrolls that can bridge the cracked parts of the graphene (as observed by AFM), helping to maintain a percolating pathway. This phenomenon of maintaining conductivity by a percolating pathway has been reported before for cracked metal or semiconductor films on elastomer substrates (*40*, *41*).

To evaluate these graphene-based films as gate electrodes in stretchable devices, we covered the graphene layer with an SEBS dielectric layer (2 μm thick) and monitored the dielectric capacitance change as a function of strain (see Fig. 2F and the Supplementary Materials for details). We observed that capacitances with plain monolayer and bilayer graphene electrodes quickly decreased because of the loss of in-plane conductivity of graphene. In contrast, capacitances gated by MGGs as well as plain trilayer graphene showed an increase of capacitance with strain, which is expected because of reduction in dielectric thickness with strain. The expected increase in capacitance matched very well with the MGG structure (fig. S8). This indicates that MGG is suitable as a gate electrode for stretchable transistors.

Exploration of CNTs as a replacement of graphene scrolls

To further investigate the role of the 1D graphene scroll on the strain tolerance of electrical conductivity and better control the separation in between graphene layers, we used spray-coated CNTs to replace the graphene scrolls (see Supplementary Materials). To mimic MGG structures, we deposited three densities of CNTs (that is, CNT1<CNT2<CNT3) on graphene, followed by another transferred graphene layer to make a G-CNT-G stack (Fig. 3, A to C). Similar to the MGG structures, G-CNT-G also exhibits a moderate increase in resistance even up to 100% strain, which is perpendicular to the direction of current flow. With a higher CNT density, the G-CNT-G stack demonstrated less resistance change with increasing strain at the expense of reduced optical transmittance (Fig. 3, D and E). This indicates that combining conductive 1D structures with transferred graphene is a general approach to improving the electrical stretchability of graphene. The advantage of graphene scrolls is that they are formed spontaneously during a transfer process without any additional processing steps. In addition, with similar film transmittance, both the conductivity and strain tolerance of MGG is better than G-CNT-G (Table 1). For example, the resistance change of G-CNT3-G is more than three times larger than that of a trilayer MGG although the transmittance is 1.1% lower than that of trilayer MGG. This implies that although intercalating conductive species in between graphene layers is a common approach toward stretchable and transparent electrodes, the MGG is better in electrical performance, transparency, and strain tolerance. This is most

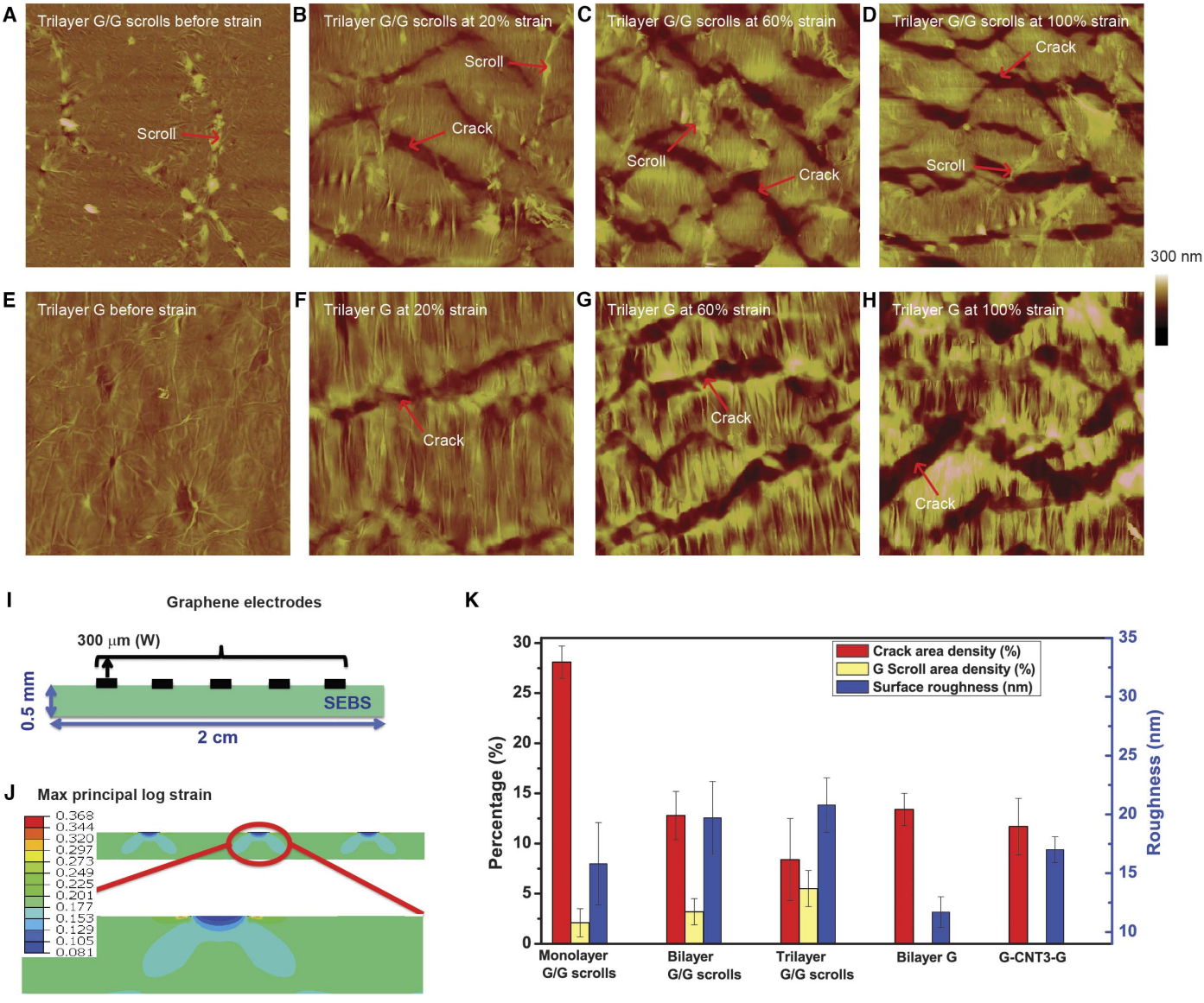

Fig. 4. Understanding the strain tolerance of conductivity of various graphene structures. (**A** to **H**) In situ AFM images of trilayer G/G scrolls (A to D) and trilayer G structures (E to H) on a very thin SEBS (~0.1 mm thick) elastomer at 0, 20, 60, and 100% strain. Representative cracks and scrolls are pointed with arrows. All the AFM images are in an area of 15 μm × 15 μm, using the same color scale bar as labeled. (**I**) Simulation geometry of patterned monolayer graphene electrodes on the SEBS substrate. (**J**) Simulation contour map of the maximal principal logarithmic strain in the monolayer graphene and the SEBS substrate at 20% external strain. (**K**) Comparison of crack area density (red column), scroll area density (yellow column), and surface roughness (blue column) for different graphene structures.

likely due to the larger dimension and higher conductivity of the graphene nanoscrolls as well as their irregular height, which is more effective in decreasing graphene layer-layer interaction and connecting the cracked graphene domains formed during strain.

Understanding the strain tolerance of conductivity of various graphene structures

To further understand their capability as electrodes for stretchable electronics, we systematically investigated the morphologies of MGG and G-CNT-G under strain. Optical microscopy and scanning electron microscopy (SEM) are not effective characterization methods because both lack color contrast and SEM is subject to image artifacts during electron scanning when graphene is on polymer substrates (figs. S9 and S10). To observe in situ the graphene surface under strain, we collected AFM measurements on trilayer MGGs and plain graphene after transferring onto very thin (~0.1 mm thick) and elastic SEBS substrates. Because of the intrinsic defects in CVD graphene and extrinsic damage during the transfer process, cracks are inevitably generated on the strained graphene, and with increasing strain, the cracks became denser (Fig. 4, A to D). Depending on the stacking structure of the carbon-based electrodes, the cracks exhibit different morphologies (fig. S11) (*27*). Crack area density (defined as crack area/analyzed area) of multilayer graphene is less than that of monolayer graphene after strain, which is consistent with the increase in electrical conductivity for MGGs. On the other hand, scrolls are often observed to bridge the cracks, providing additional conductive pathways in the strained film. For example, as labeled in the image of

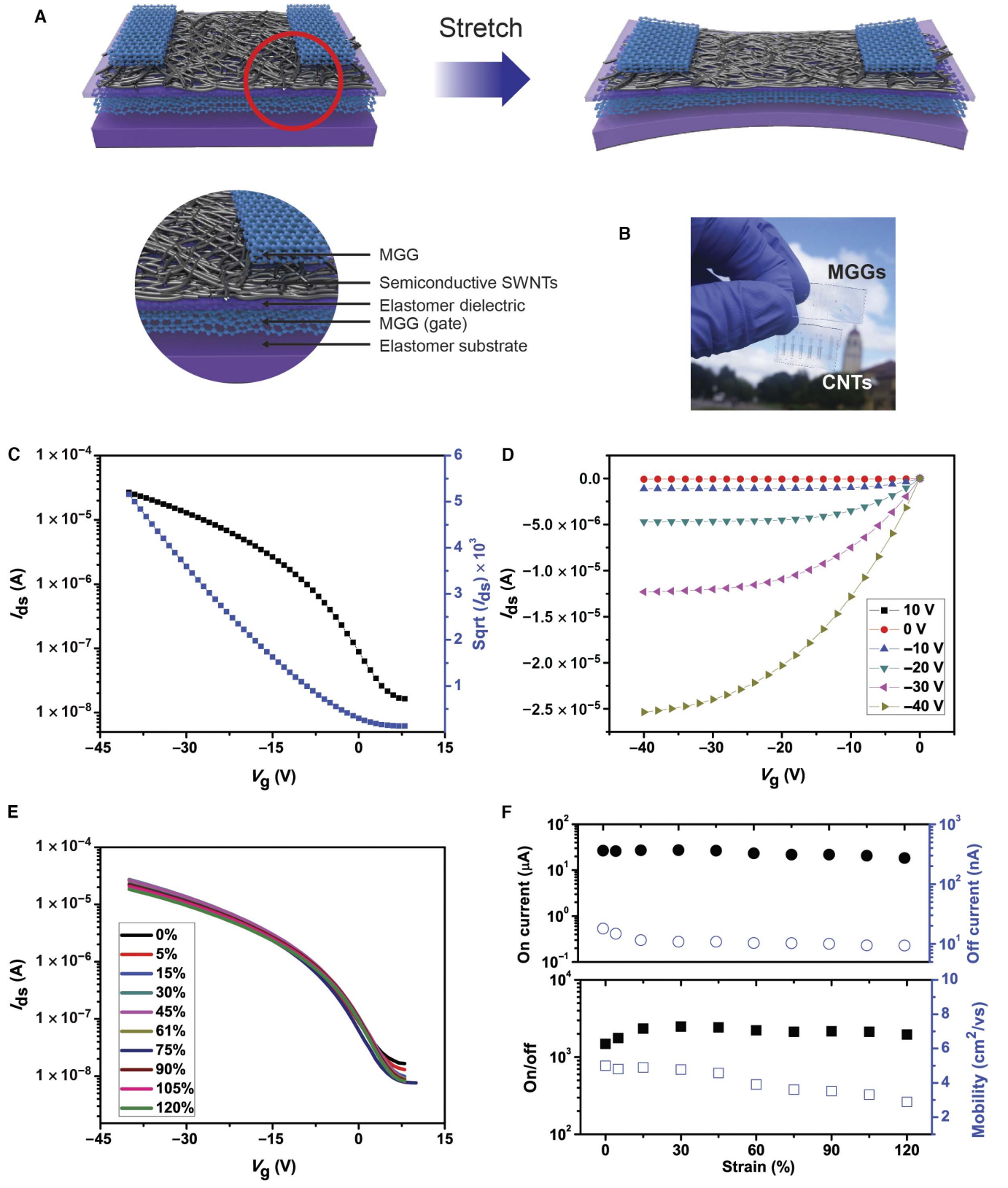

Fig. 5. Demonstration of stretchable and transparent all-carbon transistors. (**A**) Scheme of graphene-based stretchable transistor. SWNTs, single-walled carbon nanotubes. (**B**) Photo of the stretchable transistors made of graphene electrodes (top) and CNT electrodes (bottom). The difference in transparency is clearly noticeable. (**C** and **D**) Transfer and output curves of the graphene-based transistor on SEBS before strain. (**E** and **F**) Transfer curves, on and off current, on/off ratio, and mobility of the graphene-based transistor at different strains.

Fig. 4B, a wide scroll crossed over a crack in the trilayer MGG, but no scroll was observed in the plain graphene (Fig. 4, E to H). Similarly, CNTs also bridged the cracks in graphene (fig. S11). The crack area density, scroll area density, and roughness of the films are summarized in Fig. 4K.

When the MGG films are stretched, there is an important additional mechanism that the scrolls can bridge cracked regions of graphene, maintaining a percolating network. The graphene scrolls are promising because they can be tens of micrometers in length and therefore able to bridge cracks that are typically up to micrometer scale. Furthermore, because the scrolls consist of multilayers of graphene, they are expected to have low resistance. In comparison, relatively dense (lower transmittance) CNT networks are required to provide comparable conductive bridging capability, as CNTs are smaller (typically a few micrometers in length) and less conductive than scrolls. On the other hand, as shown in fig. S12, whereas the graphene cracks during stretching to accommodate strain, the scrolls do not crack, indicating that the latter might be sliding on the underlying graphene. The reason that they do not crack is likely due to the rolled-up structure, composed of many layers of graphene (~1 to 20 μm long, ~0.1 to 1 μm wide, and ~10 to 100 nm high), which has a higher effective modulus than the single-layer graphene. As reported by Green and Hersam (*42*), metallic CNT networks (tube diameter of 1.0 nm) can achieve low sheet resistances <100 ohms/sq despite the large junction resistance between CNTs. Considering that our graphene scrolls have widths of 0.1 to 1 μm and that the G/G scrolls have much larger contact areas than CNTs, the contact resistance and contact area between graphene and graphene scrolls should not be limiting factors to maintain high conductivity.

The graphene has a much higher modulus than the SEBS substrate. Although the effective thickness of the graphene electrode is much lower than that of the substrate, the stiffness of the graphene times its thickness is comparable to that of the substrate (*43*, *44*), resulting in a moderate rigid-island effect. We simulated the deformation of a 1-nm-thick graphene on an SEBS substrate (see Supplementary Materials for details). According to the simulation results, when 20% strain is applied to the SEBS substrate externally, the average strain in the graphene is ~6.6% (Fig. 4J and fig. S13D), which is consistent with experimental observations (see fig. S13). We compared the strain in the patterned graphene and substrate regions using optical microscopy and found the strain in the substrate region to be at least twice the strain in the graphene region. This indicates that the strain applied on graphene electrode patterns could be significantly confined, forming graphene stiff islands on top of SEBS (*26*, *43*, *44*).

Therefore, the ability of MGG electrodes to maintain high conductivity under high strain is likely enabled by two major mechanisms: (i) The scrolls can bridge disconnected regions to maintain a conductive percolation pathway, and (ii) the multilayer graphene sheets/elastomer may slide over each other, resulting in reduced strain on graphene electrodes. For multiple layers of transferred graphene on elastomer, the layers are not strongly attached with each other, which may slide in response to strain (*27*). The scrolls also increased the roughness of the graphene layers, which may help to increase the separation between graphene layers and therefore enable the sliding of the graphene layers.

Demonstration of stretchable and transparent all-carbon transistors

All-carbon devices are enthusiastically pursued because of low cost and high throughput. In our case, all-carbon transistors were fabricated using a bottom graphene gate, a top graphene source/drain contact, a sorted CNT semiconductor, and SEBS as a dielectric (Fig. 5A). As shown in Fig. 5B, an all-carbon device with CNTs as the source/drain and gate (bottom device) is more opaque than the device with graphene electrodes (top device). This is because CNT networks require larger thicknesses and, consequently, lower optical transmittances to achieve sheet resistances similar to that of graphene (fig. S4). Figure 5 (C and D) shows representative transfer and output curves before strain for a transistor made with bilayer MGG electrodes. The channel width and length of the unstrained transistor were 800 and 100 μm, respectively. The measured on/off ratio is greater than 10^3 with on and off currents at the levels of 10^{-5} and 10^{-8} A, respectively. The output curve exhibits ideal linear and saturation regimes with clear gate-voltage dependence, indicating ideal contact between CNTs and graphene electrodes (*45*). The contact resistance with graphene electrodes was observed to be lower than that with evaporated Au film (see fig. S14). The saturation mobility of the stretchable transistor is about 5.6 cm^2/Vs, similar to that of the same polymer-sorted CNT transistors on rigid Si substrates with 300-nm SiO_2 as a dielectric layer. Further improvement in mobility is possible with optimized tube density and other types of tubes (*46*).

When the transparent, all-carbon device was stretched in the direction parallel to the charge transport direction, minimal degradation was observed up to 120% strain. During stretching, the mobility continuously decreased from 5.6 cm^2/Vs at 0% strain to 2.5 cm^2/Vs at 120% strain (Fig. 5F). We also compared the transistor performance for different channel lengths (see table S1). Notably, at a strain as large as 105%, all these transistors still exhibited a high on/off ratio (>10^3) and mobility (>3 cm^2/Vs). In addition, we summarized all the recent work on all-carbon transistors (see table S2) (*47*–*52*). By optimizing device fabrication on elastomers and using MGGs as contacts, our all-carbon

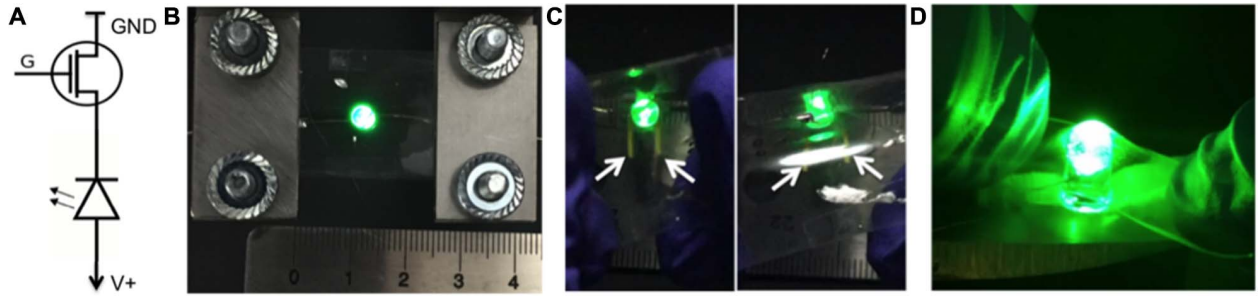

Fig. 6. Demonstration of stretchable LED control units by all-carbon transistors. (**A**) Circuit of a transistor to drive LED. GND, ground. (**B**) Photo of the stretchable and transparent all-carbon transistor at 0% strain mounted above a green LED. (**C**) The all-carbon transparent and stretchable transistor used to switch the LED is being mounted above the LED at 0% (left) and ~100% strain (right). White arrows point as the yellow markers on the device to show the distance change being stretched. (**D**) Side view of the stretched transistor, with the LED pushed into the elastomer.

transistors show good performance in terms of mobility and hysteresis as well as being highly stretchable.

As an application of the fully transparent and stretchable transistor, we used it to control an LED's switching (Fig. 6A). As shown in Fig. 6B, the green LED can be seen clearly through the stretchable all-carbon device placed directly above. While stretching to ~100% (Fig. 6, C and D), the LED light intensity does not change, which is consistent with the transistor performance described above (see movie S1). This is the first report of stretchable control units made using graphene electrodes, demonstrating a new possibility for graphene stretchable electronics.

CONCLUSION

In conclusion, we have developed a transparent conductive graphene structure that maintains high conductivity under large strains as stretchable electrodes, enabled by graphene nanoscrolls in between stacked graphene layers. These bi- and trilayer MGG electrode structures on an elastomer can maintain 21 and 65%, respectively, of their 0% strain conductivities at a strain as high as 100%, compared to complete loss of conductivity at 5% strain for typical monolayer graphene electrodes. The additional conductive paths of graphene scrolls as well as the weak interaction between the transferred layers contribute to the superior conductivity stability under strain. We further applied this graphene structure to fabricate all-carbon stretchable transistors. So far, this is the most stretchable graphene-based transistor with the best transparency without using buckling. Although the present study was conducted to enable graphene for stretchable electronics, we believe that this approach can be extended to other 2D materials to enable stretchable 2D electronics.

MATERIALS AND METHODS

Fabrication of MGG structures

Large-area CVD graphene was grown on suspended Cu foils (99.999%; Alfa Aesar) under a constant pressure of 0.5 mtorr with 50–SCCM (standard cubic centimeter per minute) CH_4 and 20–SCCM H_2 as precursors at 1000°C. Both sides of the Cu foil were covered by monolayer graphene. A thin layer of PMMA (2000 rpm; A4, Microchem) was spin-coated on one side of the Cu foil, forming a PMMA/G/Cu foil/G structure. Subsequently, the whole film was soaked in 0.1 M ammonium persulfate [$(NH_4)_2S_2O_8$] solution for about 2 hours to etch away the Cu foil. During this process, the unprotected backside graphene first tore along the grain boundaries and then rolled up into scrolls because of surface tension. The scrolls were attached onto the PMMA-supported upper graphene film, forming PMMA/G/G scrolls. The films were subsequently washed in deionized water several times and laid on a target substrate, such as a rigid SiO_2/Si or plastic substrate. As soon as the attached film dried on the substrate, the sample was sequentially soaked in acetone, 1:1 acetone/IPA (isopropyl alcohol), and IPA for 30 s each to remove PMMA. The films were heated at 100°C for 15 min or kept in a vacuum overnight to completely remove the trapped water before another layer of G/G scroll was transferred onto it. This step was to avoid the detachment of graphene film from the substrate and ensure full coverage of MGGs during the release of PMMA carrier layer.

Characterizations of MGG structures

The morphology of the MGG structure was observed using an optical microscope (Leica) and a scanning electron microscope (1 kV; FEI). An atomic force microscope (Nanoscope III, Digital Instrument) was operated in tapping mode to observe the details of the G scrolls. Film transparency was tested by an ultraviolet-visible spectrometer (Agilent Cary 6000i). For the tests when the strain was along the perpendicular direction of current flow, photolithography and O_2 plasma were used to pattern graphene structures into strips (~300 μm wide and ~2000 μm long), and Au (50 nm) electrodes were thermally deposited using shadow masks at both ends of the long side. The graphene strips were then put in contact with an SEBS elastomer (~2 cm wide and ~5 cm long), with the long axis of the strips parallel to the short side of SEBS followed by BOE (buffered oxide etch) (HF:H_2O 1:6) etching and eutectic gallium indium (EGaIn) as electrical contacts. For parallel strain tests, unpatterned graphene structures (~5 × 10 mm) were transferred onto SEBS substrates, with long axes parallel to the long side of the SEBS substrate. For both cases, the entire G (without G scrolls)/SEBS was stretched along the long side of the elastomer in a manual apparatus, and in situ, we measured their resistance changes under strain on a probe station with a semiconductor analyzer (Keithley 4200-SCS).

Fabrication of transparent stretchable all-carbon transistors

The highly stretchable and transparent all-carbon transistors on an elastic substrate were fabricated by the following procedures to avoid organic solvent damage of the polymer dielectric and substrate. MGG structures were transferred onto SEBS as gate electrodes. To obtain a uniform thin-film polymer dielectric layer (2 μm thick), a SEBS toluene (80 mg/ml) solution was spin-coated on an octadecyltrichlorosilane (OTS)–modified SiO_2/Si substrate at 1000 rpm for 1 min. The thin dielectric film can be easily transferred from the hydrophobic OTS surface onto the SEBS substrate covered with the as-prepared graphene. A capacitor could be made by depositing a liquid-metal (EGaIn; Sigma-Aldrich) top electrode to determine the capacitance as a function of strain using an LCR (inductance, capacitance, resistance) meter (Agilent). The other part of the transistor consisted of polymer-sorted semiconducting CNTs, following the procedures reported previously (*53*). The patterned source/drain electrodes were fabricated on rigid SiO_2/Si substrates. Subsequently, the two parts, dielectric/G/SEBS and CNTs/patterned G/SiO_2/Si, were laminated to each other, and soaked in BOE to remove the rigid SiO_2/Si substrate. Thus, the fully transparent and stretchable transistors were fabricated. The electrical testing under strain was performed on a manual stretching setup as the aforementioned method.

SUPPLEMENTARY MATERIALS

Supplementary material for this article is available at http://advances.sciencemag.org/cgi/content/full/3/9/e1700159/DC1

Experimental section

Additional supporting information

fig. S1. Optical microscopy images of monolayer MGG on SiO_2/Si substrates at different magnifications.

fig. S2. SEM images of mono-, bi-, and trilayer MGGs on the SiO_2/Si wafers.

fig. S3. SEM images of graphene film covered with spray-coated CNTs.

fig. S4. Comparison of two-probe sheet resistances and transmittances @550 nm of mono-, bi- and trilayer plain graphene (black squares), MGG (red circles), and CNTs (blue triangle).

fig. S5. Sheet resistances of mono-, bi-, and trilayer MGGs.

fig. S6. Optical transmittances of MGGs and multilayer plain graphene.

fig. S7. Normalized resistance change of mono- and bilayer MGGs (black) and G (red) under ~1000 cyclic strain loading up to 40 and 90% parallel strain, respectively.

fig. S8. Calculation of relative areal capacitance change as a function of strain.

fig. S9. Optical microscopy image of trilayer MGG on SEBS elastomer.

fig. S10. SEM image of trilayer MGG on SEBS elastomer after strain, showing a long scroll cross over several cracks.

fig. S11. AFM images of various graphene structures on SEBS elastomer after 100% strain.

fig. S12. AFM image of trilayer MGG on very thin SEBS elastomer at 20% strain, showing that a scroll crossed over a crack.
fig. S13. Optical microscopy observation and simulation of graphenes on SEBS under strain.
fig. S14. Contact resistances of monolayer G/CNTs and Au/CNTs at different gate voltages.
table S1. Mobilities of bilayer MGG–single-walled carbon nanotube transistors at different channel lengths before and after strain.
table S2. Summary of recent work on all-carbon transistors.
movie S1. Demonstration of stretchable LED control units by all-carbon transistors.
References (*54*–*58*)

REFERENCES AND NOTES

1. D. Kuzum, H. Takano, E. Shim, J. C. Reed, H. Juul, A. G. Richardson, J. de Vries, H. Bink, M. A. Dichter, T. H. Lucas, D. A. Coulter, E. Cubukcu, B. Litt, Transparent and flexible low noise graphene electrodes for simultaneous electrophysiology and neuroimaging. *Nat. Commun.* **5**, 5259 (2014).
2. S. J. Kim, K. W. Cho, H. R. Cho, L. Wang, S. Y. Park, S. E. Lee, T. Hyeon, N. Lu, S. H. Choi, D.-H. Kim, Stretchable and transparent biointerface using cell-sheet–graphene hybrid for electrophysiology and therapy of skeletal muscle. *Adv. Funct. Mater.* **26**, 3207–3217 (2016).
3. J. Liang, L. Li, X. Niu, Z. Yu, Q. Pei, Elastomeric polymer light-emitting devices and displays. *Nat. Photonics* **7**, 817–824 (2013).
4. S. Li, B. N. Peele, C. M. Larson, H. Zhao, R. F. Shepherd, A stretchable multicolor display and touch interface using photopatterning and transfer printing. *Adv. Mater.* **28**, 9770–9775 (2016).
5. S. Bae, H. Kim, Y. Lee, X. Xu, J.-S. Park, Y. Zheng, J. Balakrishnan, T. Lei, H. R. Kim, Y. I. Song, Y.-J. Kim, K. S. Kim, B. Özyilmaz, J.-H. Ahn, B. H. Hong, S. Iijima, Roll-to-roll production of 30-inch graphene films for transparent electrodes. *Nat. Nanotechnol.* **5**, 574–578 (2010).
6. X. Li, Y. Zhu, W. Cai, M. Borysiak, B. Han, D. Chen, R. D. Piner, L. Colombo, R. S. Ruoff, Transfer of large-area graphene films for high-performance transparent conductive electrodes. *Nano Lett.* **9**, 4359–4363 (2009).
7. D. R. Cairns, R. P. Witte II, D. K. Sparacin, S. M. Sachsman, D. C. Paine, G. P. Crawford, Strain-dependent electrical resistance of tin-doped indium oxide on polymer substrates. *Appl. Phys. Lett.* **76**, 1425 (2000).
8. K. S. Kim, Y. Zhao, H. Jang, S. Y. Lee, J. M. Kim, K. S. Kim, J.-H. Ahn, P. Kim, J.-Y. Choi, B. H. Hong, Large-scale pattern growth of graphene films for stretchable transparent electrodes. *Nature* **457**, 706–710 (2009).
9. H. Lee, I. Kim, M. Kim, H. Lee, Moving beyond flexible to stretchable conductive electrodes using metal nanowires and graphenes. *Nanoscale* **8**, 1789–1822 (2016).
10. T.-K. Hong, D. W. Lee, H. J. Choi, H. S. Shin, B.-S. Kim, Transparent, flexible conducting hybrid multilayer thin films of multiwalled carbon nanotubes with graphene nanosheets. *ACS Nano* **4**, 3861–3868 (2010).
11. V. C. Tung, L.-M. Chen, M. J. Allen, J. K. Wassei, K. Nelson, R. B. Kaner, Y. Yang, low-temperature solution processing of graphene–carbon nanotube hybrid materials for high-performance transparent conductors. *Nano Lett.* **9**, 1949–1955 (2009).
12. D. Jariwala, T. J. Marks, M. C. Hersam, Mixed-dimensional van der Waals heterostructures. *Nat. Mater.* **16**, 170–181 (2017).
13. X. Wan, G. Long, L. Huang, Y. Chen, Graphene—A promising material for organic photovoltaic cells. *Adv. Mater.* **23**, 5342–5358 (2011).
14. L. Britnell, R. V. Gorbachev, R. Jalil, B. D. Belle, F. Schedin, A. Mishchenko, T. Georgiou, M. I. Katsnelson, L. Eaves, S. V. Morozov, N. M. R. Peres, J. Leist, A. K. Geim, K. S. Novoselov, L. A. Ponomarenko, Field-effect tunneling transistor based on vertical graphene heterostructures. *Science* **335**, 947–950 (2012).
15. T. Georgiou, R. Jalil, B. D. Belle, L. Britnell, R. V. Gorbachev, S. V. Morozov, Y.-J. Kim, A. Gholinia, S. J. Haigh, O. Makarovsky, L. Eaves, L. A. Ponomarenko, A. K. Geim, K. S. Novoselov, A. Mishchenko, Vertical field-effect transistor based on graphene–WS_2 heterostructures for flexible and transparent electronics. *Nat. Nanotechnol.* **8**, 100–103 (2013).
16. K. S. Novoselov, V. I. Fal'ko, L. Colombo, P. R. Gellert, M. G. Schwab, K. Kim, A roadmap for graphene. *Nature* **490**, 192–200 (2012).
17. H. Jang, Y. J. Park, X. Chen, T. Das, M.-S. Kim, J.-H. Ahn, Graphene-based flexible and stretchable electronics. *Adv. Mater.* **28**, 4184–4202 (2015).
18. F. Bonaccorso, Z. Sun, T. Hasan, A. C. Ferrari, Graphene photonics and optoelectronics. *Nat. Photonics* **4**, 611–622 (2010).
19. X. Huang, Z. Zeng, Z. Fan, J. Liu, H. Zhang, Graphene-based electrodes. *Adv. Mater.* **24**, 5979–6004 (2012).
20. S.-K. Lee, H. Y. Jang, S. Jang, E. Choi, B. H. Hong, J. Lee, S. Park, J.-H. Ahn, All graphene based thin film transistors on flexible plastic substrates. *Nano Lett.* **12**, 3472–3476 (2012).
21. T.-H. Han, Y. Lee, M.-R. Choi, S.-H. Woo, S.-H. Bae, B. H. Hong, J.-H. Ahn, T.-W. Lee, Extremely efficient flexible organic light-emitting diodes with modified graphene anode. *Nat. Photonics* **6**, 105–110 (2012).
22. J. Lee, T.-H. Han, M.-H. Park, D. Y. Jung, J. Seo, H.-K. Seo, H. Cho, E. Kim, J. Chung, S.-Y. Choi, T.-S. Kim, T.-W. Lee, S. Yoo, Synergetic electrode architecture for efficient graphene-based flexible organic light-emitting diodes. *Nat. Commun.* **7**, 11791 (2016).
23. T.-H. Han, S.-J. Kwon, N. Li, H.-K. Seo, W. Xu, K. S. Kim, T.-W. Lee, Versatile p-type chemical doping to achieve ideal flexible graphene electrodes. *Angew. Chem. Int. Ed. Engl.* **55**, 6197–6201 (2016).
24. B. W. An, B. G. Hyun, S.-Y. Kim, M. Kim, M.-S. Lee, K. Lee, J. B. Koo, H. Y. Chu, B.-S. Bae, J.-U. Park, Stretchable and transparent electrodes using hybrid structures of graphene–metal nanotrough networks with high performances and ultimate uniformity. *Nano Lett.* **14**, 6322–6328 (2014).
25. S. H. Chae, W. J. Yu, J. J. Bae, D. L. Duong, D. Perello, H. Y. Jeong, Q. H. Ta, T. H. Ly, Q. A. Vu, M. Yun, X. Duan, Y. H. Lee, Transferred wrinkled Al_2O_3 for highly stretchable and transparent graphene–carbon nanotube transistors. *Nat. Mater.* **12**, 403–409 (2013).
26. R. J. T. Nicholl, H. J. Conley, N. V. Lavrik, I. Vlassiouk, Y. S. Puzyrev, V. P. Sreenivas, S. T. Pantelides, K. I. Bolotin, The effect of intrinsic crumpling on the mechanics of free-standing graphene. *Nat. Commun.* **6**, 8789 (2015).
27. S. Won, Y. Hwangbo, S.-K. Lee, K.-S. Kim, K.-S. Kim, S.-M. Lee, H.-J. Lee, J.-H. Ahn, J.-H. Kim, S.-B. Lee, Double-layer CVD graphene as stretchable transparent electrodes. *Nanoscale* **6**, 6057–6064 (2014).
28. K.-Y. Chun, Y. Oh, J. Rho, J.-H. Ahn, Y.-J. Kim, H. R. Choi, S. Baik, Highly conductive, printable and stretchable composite films of carbon nanotubes and silver. *Nat. Nanotechnol.* **5**, 853–857 (2010).
29. N. Matsuhisa, M. Kaltenbrunner, T. Yokota, H. Jinno, K. Kuribara, T. Sekitani, T. Someya, Printable elastic conductors with a high conductivity for electronic textile applications. *Nat. Commun.* **6**, 7461 (2015).
30. M. Kaltenbrunner, G. Adam, E. D. Głowacki, M. Drack, R. Schwödiauer, L. Leonat, D. H. Apaydin, H. Groiss, M. C. Scharber, M. S. White, N. S. Sariciftci, S. Bauer, Flexible high power-per-weight perovskite solar cells with chromium oxide–metal contacts for improved stability in air. *Nat. Mater.* **14**, 1032–1039 (2015).
31. J. Viventi, D.-H. Kim, L. Vigeland, E. S. Frechette, J. A. Blanco, Y.-S. Kim, A. E. Avrin, V. R. Tiruvadi, S.-W. Hwang, A. C. Vanleer, D. F. Wulsin, K. Davis, C. E. Gelber, L. Palmer, J. Van der Spiegel, J. Wu, J. Xiao, Y. Huang, D. Contreras, J. A. Rogers, B. Litt, Flexible, foldable, actively multiplexed, high-density electrode array for mapping brain activity in vivo. *Nat. Neurosci.* **14**, 1599–1605 (2011).
32. S.-K. Lee, B. J. Kim, H. Jang, S. C. Yoon, C. Lee, B. H. Hong, J. A. Rogers, J. H. Cho, J.-H. Ahn, Stretchable graphene transistors with printed dielectrics and gate electrodes. *Nano Lett.* **11**, 4642–4646 (2011).
33. T. Yamada, Y. Hayamizu, Y. Yamamoto, Y. Yomogida, A. Izadi-Najafabadi, D. N. Futaba, K. Hata, A stretchable carbon nanotube strain sensor for human-motion detection. *Nat. Nanotechnol.* **6**, 296–301 (2011).
34. N. Lu, C. Lu, S. Yang, J. Rogers, Highly sensitive skin-mountable strain gauges based entirely on elastomers. *Adv. Funct. Mater.* **22**, 4044–4050 (2012).
35. M. K. Blees, A. W. Barnard, P. A. Rose, S. P. Roberts, K. L. McGill, P. Y. Huang, A. R. Ruyack, J. W. Kevek, B. Kobrin, D. A. Muller, P. L. McEuen, Graphene kirigami. *Nature* **524**, 204–207 (2015).
36. O. V. Yazyev, S. G. Louie, Topological defects in graphene: Dislocations and grain boundaries. *Phys. Rev. B Condens. Matter Mater. Phys.* **81**, 195420 (2010).
37. B. Wang, Y. S. Puzyrev, S. T. Pantelides, Enhanced chemical reactions of oxygen at grain boundaries in polycrystalline graphene. *Polyhedron* **64**, 158–162 (2013).
38. X. Xie, L. Ju, X. Feng, Y. Sun, R. Zhou, K. Liu, S. Fan, Q. Li, K. Jiang, Controlled fabrication of high-quality carbon nanoscrolls from monolayer graphene. *Nano Lett.* **9**, 2565–2570 (2009).
39. L. M. Viculis, J. J. Mack, R. B. Kaner, A chemical route to carbon nanoscrolls. *Science* **299**, 1361 (2003).
40. I. M. Graz, D. P. J. Cotton, S. P. Lacour, Extended cyclic uniaxial loading of stretchable gold thin-films on elastomeric substrates. *Appl. Phys. Lett.* **94**, 071902 (2009).
41. A. Chortos, J. Lim, J W. F. To, M. Vosgueritchian, T. J. Dusseault, T.-H. Kim, S. Hwang, Z. Bao, Highly stretchable transistors using a microcracked organic semiconductor. *Adv. Mater.* **26**, 4253–4259 (2014).
42. A. A. Green, M. C. Hersam, Colored semitransparent conductive coatings consisting of monodisperse metallic single-walled carbon nanotubes. *Nano Lett.* **8**, 1417–1422 (2008).
43. R. Faccio, P. A. Denis, H. Pardo, C. Goyenola, A. W. Mombrú, Mechanical properties of graphene nanoribbons. *J. Phys. Condens. Matter* **21**, 285304 (2009).
44. C. Lee, X. Wei, J. W. Kysar, J. Hone, Measurement of the elastic properties and intrinsic strength of monolayer graphene. *Science* **321**, 385–388 (2008).
45. C.-a. Di, D. Wei, G. Yu, Y. Liu, Y. Guo, D. Zhu, Patterned graphene as source/drain electrodes for bottom-contact organic field-effect transistors. *Adv. Mater.* **20**, 3289–3293 (2008).

46. T. Lei, G. Pitner, X. Chen, G. Hong, S. Park, P. Hayoz, R. T. Weitz, H.-S. P. Wong, Z. Bao, Dispersion of high-purity semiconducting arc-discharged carbon nanotubes using backbone engineered diketopyrrolopyrrole (DPP)-based polymers. *Adv. Electron. Mater.* **2**, 1500299 (2016).
47. M. Xia, Z. Cheng, J. Han, S. Zhang, Extremely stretchable all-carbon-nanotube transistor on flexible and transparent substrates. *Appl. Phys. Lett.* **105**, 143504 (2014).
48. F. Xu, M.-Y. Wu, N. S. Safron, S. S. Roy, R. M. Jacobberger, D. J. Bindl, J.-H. Seo, T.-H. Chang, Z. Ma, M. S. Arnold, Highly stretchable carbon nanotube transistors with ion gel gate dielectrics. *Nano Lett.* **14**, 682–686 (2014).
49. L. Cai, S. Zhang, J. Miao, Z. Yu, C. Wang, Fully printed stretchable thin-film transistors and integrated logic circuits. *ACS Nano* **10**, 11459–11468 (2016).
50. A. Chortos, G. I. Koleilat, R. Pfattner, D. Kong, P. Lin, R. Nur, T. Lei, H. Wang, N. Liu, Y.-C. Lai, M.-G. Kim, J. W. Chung, S. Lee, Z. Bao, Mechanically durable and highly stretchable transistors employing carbon nanotube semiconductor and electrodes. *Adv. Mater.* **28**, 4441–4448 (2016).
51. J. Liang, L. Li, D. Chen, T. Hajagos, Z. Ren, S.-Y. Chou, W. Hu, Q. Pei, Intrinsically stretchable and transparent thin-film transistors based on printable silver nanowires, carbon nanotubes and an elastomeric dielectric. *Nat. Commun.* **6**, 7647 (2015).
52. A. Sekiguchi, F. Tanaka, T. Saito, Y. Kuwahara, S. Sakurai, D. N. Futaba, T. Yamada, K. Hata, Robust and soft elastomeric electronics tolerant to our daily lives. *Nano Lett.* **15**, 5716–5723 (2015).
53. T. Lei, X. Chen, G. Pitner, H.-S. P. Wong, Z. Bao, Removable and recyclable conjugated polymers for highly selective and high-yield dispersion and release of low-cost carbon nanotubes. *J. Am. Chem. Soc.* **138**, 802–805 (2016).
54. P. I. Hsu, R. Bhattacharya, H. Gleskova, M. Huang, Z. Xi, Z. Suo, S. Wagner, J. C. Sturmless, Thin-film transistor circuits on large-area spherical surfaces. *Appl. Phys. Lett.* **81**, 1723–1725 (2002).
55. J. A. Rogers, T. Someya, Y. Huang, Materials and mechanics for stretchable electronics. *Science* **327**, 1603–1607 (2010).
56. J. Song, Mechanics of stretchable electronics. *Curr. Opin. Solid State Mater. Sci.* **19**, 160–170 (2015).
57. J. Dargahi, S. Najarian, Human tactile perception as a standard for artificial tactile sensing—A review. *Int. J. Med. Robot.* **1**, 23–35 (2004).
58. N. C. Chen, P. H. Chang, A. P. Chiu, M. C. Wang, W. S. Feng, G. M. Wu, C. F. Shih, K. S. Liu, Modified transmission line model and its application to aluminum ohmic contacts with *n*-type GaN. *Appl. Phys. Lett.* **84**, 2584–2586 (2004).

Acknowledgments: M. Gebbie, M. Ferro, and N. Melosh at Stanford University gave advice on conductive AFM. H. Tian and H. Wang at the University of California, Los Angeles, provided part of the graphene sample on Cu foil. **Funding:** Z.B. acknowledges the support from Samsung Electronics and Air Force Office of Scientific Research (grant no. FA9550-15-1-0106). R.P. acknowledges support from the Marie Curie Cofund, Beatriu de Pinós fellowship (Agència de Gestió d' Ajuts Universitaris i de Recerca, 2014 BP-A 00094). **Author contributions:** N.L. and Z.B. conceived the idea. N.L., A.C., and T.L. performed the experiments. N.L., A.C., T.L., L.J., T.R.K., R.S., W.-G.B., C.Z., S.W., R.P., X.C., and Z.B. analyzed the data. N.L., A.C., L.J., and Z.B. wrote the paper. **Competing interests:** The authors declare that they have no competing interests. **Data and materials availability:** All data needed to evaluate the conclusions in the paper are present in the paper and/or the Supplementary Materials. Additional data related to this paper may be requested from the authors by emailing Z.B. at zbao@stanford.edu.

Submitted 15 January 2017
Accepted 9 August 2017
Published 8 September 2017
10.1126/sciadv.1700159

Citation: N. Liu, A. Chortos, T. Lei, L. Jin, T. R. Kim, W.-G. Bae, C. Zhu, S. Wang, R. Pfattner, X. Chen, R. Sinclair, Z. Bao, Ultratransparent and stretchable graphene electrodes. *Sci. Adv.* **3**, e1700159 (2017).

Science Advances

Ultratransparent and stretchable graphene electrodes

Nan Liu, Alex Chortos, Ting Lei, Lihua Jin, Taeho Roy Kim, Won-Gyu Bae, Chenxin Zhu, Sihong Wang, Raphael Pfattner, Xiyuan Chen, Robert Sinclair and Zhenan Bao

Sci Adv **3** (9), e1700159.
DOI: 10.1126/sciadv.1700159